INTERNATIONAL JOURNAL OF AUTOMOTIVE AND MECHANICAL ENGINEERING (IJAME)
ISSN: 2229-8649 e-ISSN: 2180-1606
VOL. 19, ISSUE 1, 9362 – 9378
DOI: https://doi.org/10.15282/ijame.19.1.2022.01.0720

ORIGINAL ARTICLE

Genetic Algorithm for Sensitivity Analysis of Automobile Hood Four-bar Mechanism Synthesis Using Motion Generation

Y. M. Al-Smadi[1,*], Y. Aburmaileh[1], K. Russel[2] and R. Sodhi[2]

[1]Department of Mechanical Engineering, Jordan University of Science and Technology, 22110 Irbid, Jordan
[2]Department of Mechanical and Industrial Engineering, New Jersey Institute of Technology, Newark, 07104 New Jersey, USA

ABSTRACT – In four-bar motion generation, linkage dimensions are calculated to achieve prescribed coupler positions. This work investigates the sensitivity of four-bar coupler motion sequences by analyzing position error margins and implementing a genetic algorithm (GA) for four-bar motion generation. As an application, the four-bar hood mechanism in the Plymouth Satellite mid-size automobile is considered. The results of the sensitivity analysis show that the mean average structural error between the prescribed and achieved hood positions is less than 0.015in for any quadratic analysis. In each demonstration, the proposed method consistently produced results that are scalable for 360° within a margin error of 0.06in.

ARTICLE HISTORY
Received: 7th June 2021
Revised: 9th Oct 2021
Accepted: 31st Jan 2022

KEYWORDS
Motion generation;
Four-bar mechanism;
Genetic algorithm;
Sensitivity analysis;
Vehicle hood synthesis

INTRODUCTION

The objective of four-bar motion generation is to calculate the mechanism parameters required to achieve or approximate a set of prescribed coupler positions. This mechanism design objective is particularly useful when the rigid body must achieve a specific displacement sequence for effective operation (e.g., specific tool paths and/or orientations for accurate fabrication operations). In Figure 1, the automobile hood is a part of a four-bar mechanism. The hood is the coupler that is connected between the two moving pivots and the automobile body. Work was presented for the car hood mechanism with focuses on dimensional analysis, synthesis considering three spring configurations and synthesis to reduce actuator force/torque requirement [1-3]. Ko and Yu studied the dynamic behavior of the hood mechanism furnished with gas lifter and torsion bars [4]. Untaroiu et al. studied the hood mechanism under extreme impulsive forces (i.e. crash load) [5]. Russell et al. explain the mechanism synthesis procedure for four-bar mechanisms similar to automobile hood [6]. The finite motion of the automobile hood in this work will be coupled with sensitivity analysis and genetic algorithm optimization to calculate the mechanism solution that achieves the prescribed motion.

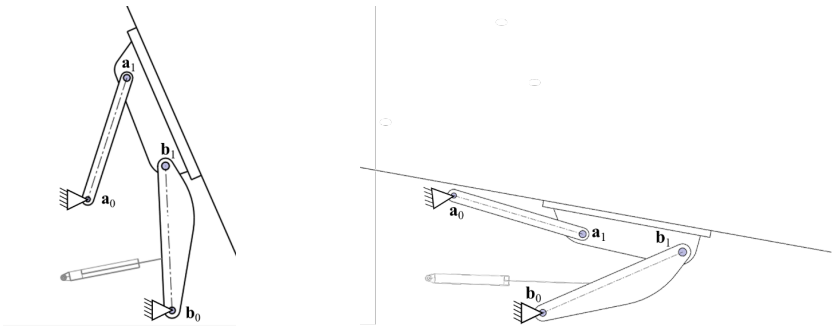

(a) (b)

Figure 1. Schematic diagram for automobile hood four-bar mechanism, (a) hood in open position and (b) hood in closed position

Almost all techniques for mechanism syntheses rely on nonlinear optimization methods with the main focus on objective function. A few examples of methods that use probabilistic nonlinear optimization (PNO) are differential evolution, GA-Fuzzy Logic and exact point synthesis [7-9]. The synthesized four-bar mechanism using PNO is far more accurate than using conventional or deterministic synthesis techniques. In these PNO methods, approximate optimal solutions are achieved by minimizing the objective function. The optimal solution is then compared to the prescribed or desired path in what is called scalar error or structural error. Traditional optimization techniques such as sequential quadratic programming (SQP), Newton-Raphson and quasi-Newton produce a noticeable scalar error or, alternatively, structural error as shown in authors' work [10-12].

*CORRESPONDING AUTHOR | Yahia M. Al-Smadi | ymsmadi@just.edu.jo

Genetic algorithm (GA) is a probabilistic optimization technique used for finding solutions based on the natural selection of chromosomes and genes. In the case of mechanism synthesis, the chromosome is the potential solution and the gene is the mechanism parameter (e.g. moving and fixed pivots). GA is also a random search technique that always looks for the fittest chromosome (candidate solution) through the process of initial populations (initial guesses). then combinations and permutations of all genes (mechanism parameters) that fit the fitness function (i.e. objective function). This optimization search process makes it very robust for solving complex problems. Many researchers used GA to synthesize four-bar mechanisms. Roston and Sturges used GA optimization to remove the limitation of using the four-bar mechanism to some real-world problems with precision points [13]. Followed by the work of Cabrera et at. and Shete et al. where GA optimization was used to synthesize the objective function of closed-loop four-bar mechanism [14-15]. Bajpai stated that GA must be handled with care otherwise premature solutions, which can produce a local minimum, can be formed [16].

The scope of this work is to synthesize the automobile hood four-bar mechanism based on the sensitivity of the coupler points. The tolerance value of the coupler points **p**, **q**, and **r** will be an input in addition to the prescribed coupler points themselves. The objective function of the fitness function, sensitivity constraints and structural error will be formulated and incorporated within the genetic algorithm, as described in Section 4. The authors' previous work used deterministic methods where a number of coupler poses are prescribed to synthesize the four-bar mechanism using the Newton Raphson technique [10-12]. Unlike the dimensional analysis methods, probabilistic methods such as GA optimization incorporate an indefinite number of prescribed rigid-body poses [13-18]. The results achieved by GA are more accurate and robust even for complex problems.

GA optimization has also been used in combination with other methods. Lin tested a new evolutionary algorithm on a four-bar linkage for path synthesis [19]. He combined the differential evolution (DE) with the real-valued GA (RGA). GA–DE hybrid algorithm differs in the content of the crossover and showed more accurate solutions than with just RGA. A combined GA–fuzzy logic method was proposed to solve a mechanism synthesis in path generation [20]. GA–FL monitored the variation of variables during the first run of GA and modified the initial bounding intervals to restart the second round of GA. Unlike these techniques, the significance of this work is to formulate sensitivity constraints that measure the robustness of the optimal solution and incorporate these constraints in the GA optimization technique for the synthesis of four-bar motion generation mechanism synthesis.

The motion generation model input includes the planar Cartesian coordinates of variables **p**, **q**, and **r** which define five prescribed rigid-body poses, as in Figure 2(a). The model output includes the x and y- components of fixed pivots $\mathbf{a_0}$ and $\mathbf{b_0}$ and moving pivot $\mathbf{a_1}$ and $\mathbf{b_1}$ of the planar four-bar motion generator, as in Figure 2(b).

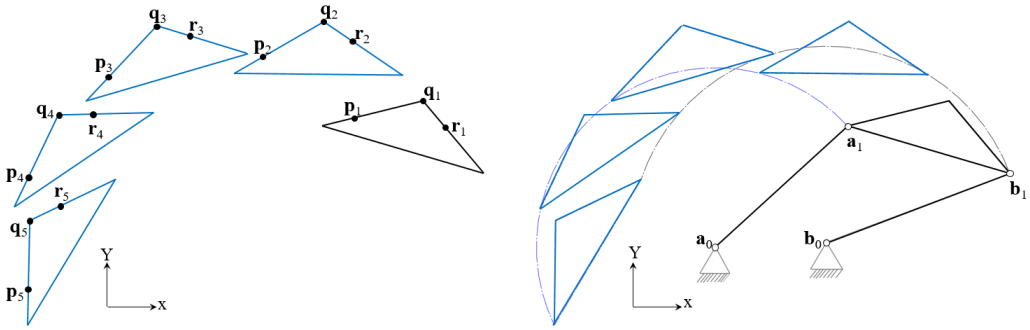

(a) (b)

Figure 2. (a) Prescribed rigid-body poses and (b) calculated planar four-bar mechanism.

MECHANISM SYNTHESIS USING PLANAR FOUR-BAR MOTION GENERATION

Equations (1) and (2) are constant length crank and follower length constraints which are incorporated in the numerical planar four-bar motion generation model [21].

$$([D_{1i}]a_1 - a_0)^T([D_{1i}]a_1 - a_0) - {L_1}^2 = 0 \tag{1}$$

$$([D_{1i}]b_1 - b_0)^T([D_{1i}]b_1 - b_0) - {L_3}^2 = 0 \tag{2}$$

where

$$[\boldsymbol{D_{1i}}] = \begin{bmatrix} \boldsymbol{p_{ix}} & \boldsymbol{q_{ix}} & \boldsymbol{r_{ix}} \\ \boldsymbol{p_{iy}} & \boldsymbol{q_{iy}} & \boldsymbol{r_{iy}} \\ \mathbf{1} & \mathbf{1} & \mathbf{1} \end{bmatrix} \begin{bmatrix} \boldsymbol{p_{1x}} & \boldsymbol{q_{1x}} & \boldsymbol{r_{1x}} \\ \boldsymbol{p_{1y}} & \boldsymbol{q_{1y}} & \boldsymbol{r_{1y}} \\ \mathbf{1} & \mathbf{1} & \mathbf{1} \end{bmatrix}^{-1} ,i = 2\text{-}5 \tag{3}$$

Equation (3) is a planar rigid-body displacement matrix resulting from direct inversion between the initial coupler position (position 1) and the displaced position (position j).

The given motion generation model is to calculate the components of the fixed pivots $\mathbf{a}_0$ and $\mathbf{b}_0$, (where $\mathbf{a}_0=[a_{0x}, a_{0y},$

1]^T, and $\mathbf{b}_0$=[b_{0x}, b_{0y}, 1]^T) and moving pivots $\mathbf{a}_1$ and $\mathbf{b}_1$ (where $\mathbf{a}_1$=[a_{1x}, a_{1y}, 1]^T, and $\mathbf{b}_1$=[b_{1x}, b_{1y}, 1]^T) of a planar four-bar motion generator in Figure 2(b). As presented, the user can specify a maximum of five rigid body poses in the motion generation model [21].

SENSITIVITY ANALYSIS

Denizhan and Chew used the sensitivity analysis to determine how the variables of a mechanism applied in conjunction with extension, compression or torsion springs linked between the vehicle body and hood are influential on the designed mechanism [2]. Hanzaki et al. performed a combination of kinematic and sensitivity optimization of a rack-and-pinion steering linkage used in passenger cars [22]. Karamoozian et al. proposed a method to compute the kinematic variations with respect to the critical dimensions (joint clearances) considering the tolerance sensitivity of mechanism for clearance in the joints in different motion phases [23]. Sancibrian synthesized a four-bar mechanism for path generation based on sensitivity analysis, which gives valuable information about the importance of each link [24]. Faik and Erdman demonstrated the sensitivity to tolerances of four-bar linkage link angles [25].

Sensitivity indices related to the variations in the locations of the four-bar mechanism's pivots $\mathbf{a}_0$, $\mathbf{b}_0$, $\mathbf{a}_1$, and $\mathbf{b}_1$ and in **p**, **q** and **r** are shown in Figure 3. The sensitivity analysis will be illustrated in one point (**q**) and then it can be applied in **p** and **r** points. Terms F_b and F_q are the base and the moving frames of the mechanism. As F_{qx} and $\mathbf{a_1b_1}$ are parallel, θ_3 is the angle between frames F_b and F_q.

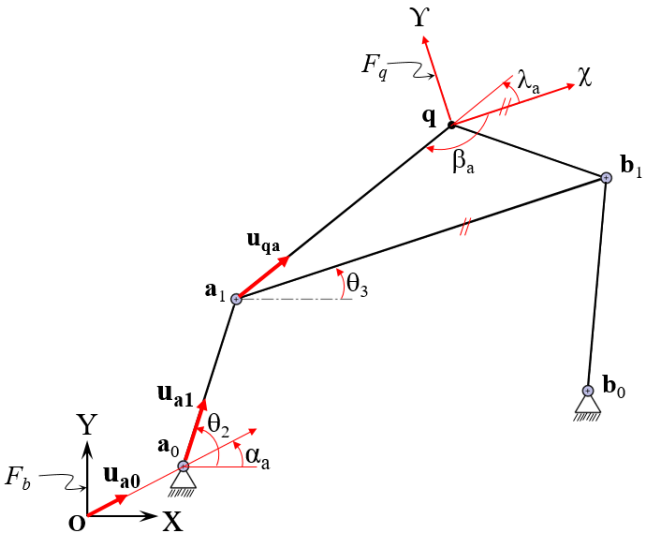

Figure 3. The architecture of the four-bar mechanism.

Sensitivity Coefficients

The base frame F_b represents the global coordinate system located at center O and the mechanism can be located on different coordinate F_q. From the closed-loop kinematic chain **O_ a₀ _ a₁_q_O** (in Figure 3), the expression of the position vector **Oq** of point **q** in the base frame (i.e. global coordinates) can be derived as the following:

$$\boldsymbol{Oa_0} + \boldsymbol{a_0a_1} + \boldsymbol{a_1q} + \boldsymbol{qO} = \mathbf{0} \tag{4a}$$

$$\boldsymbol{Oa_0} + \boldsymbol{a_0a_1} + \boldsymbol{a_1q} = \boldsymbol{Oq} = \boldsymbol{q} \tag{4b}$$

$$\boldsymbol{q} = \begin{bmatrix} q_x \\ q_y \end{bmatrix} = \boldsymbol{Oa_0} + \boldsymbol{a_0a_1} + \boldsymbol{a_1q} \tag{4c}$$

it can be expressed as

$$\boldsymbol{q} = v_{a_0}\boldsymbol{u_{a_0}} + v_{a_1}\boldsymbol{u_{a_1}} + v_q\boldsymbol{u_q} \tag{5}$$

with

$$\boldsymbol{u_{a_0}} = \begin{bmatrix} cos\,\alpha \\ sin\,\alpha \end{bmatrix}, \boldsymbol{u_{a_1}} = \begin{bmatrix} cos\,\theta_2 \\ sin\,\theta_2 \end{bmatrix}, \boldsymbol{u_q} = \begin{bmatrix} cos(\theta_3 + \beta + \pi) \\ sin(\theta_3 + \beta + \pi) \end{bmatrix}$$

where v_{a_0} is the distance between points **O** and $\mathbf{a_0}$, v_{a_1} is the distance between points $\mathbf{a_0}$ and $\mathbf{a_1}$ v_q is the distance between points $\mathbf{a_1}$ and **q**, $\boldsymbol{u_{a_0}}$ is the unit vector of vector $\mathbf{Oa_0}$, which is $\frac{\boldsymbol{Oa_0}}{|\boldsymbol{Oa_0}|}$, $\boldsymbol{u_{a_1}}$ is the unit vector of vector $\mathbf{a_0a_1}$, which is $\frac{\boldsymbol{a_0a_1}}{|\boldsymbol{a_0a_1}|}$, $\boldsymbol{u_q}$ is the unit vector of vector $\mathbf{a_1q}$, which is $\frac{\boldsymbol{a_1q}}{|\boldsymbol{a_1q}|}$. Differentiating Eq. (5) gets us the following:

$$\delta\boldsymbol{q} = \delta v_{a_0}\boldsymbol{u_{a_0}} + v_{a_0}\delta\alpha\boldsymbol{E}\boldsymbol{u_{a_0}} + \delta v_{a_1}\boldsymbol{u_{a_1}} + v_{a_1}\delta\theta_2\boldsymbol{E}\boldsymbol{u_{a_1}} + \delta v_q\boldsymbol{u_q} + v_q(\delta\theta_3 + \delta\beta)\,\boldsymbol{E}\boldsymbol{u_q} \tag{6}$$

where E is defined as $E = \begin{bmatrix} 0 & -1 \\ 1 & 0 \end{bmatrix}$

$\delta q$and $\delta\theta_3$ are the position and orientation errors of point **q** on the coupler. Likewise,δv_{a_0} ,$\delta\alpha$,δv_{a_1} , δv_q and $\delta\beta$ indicate the variations inv_{a_0},α,v_{a_1}, $v_q$andβ respectively.

The useless variation $\delta\theta_2$is eliminated by dot-multiplying Eq. (6) by $v_{a_1}\boldsymbol{u}_{\boldsymbol{a_1}}^T$. Using the same procedure for another closed-loop kinematic chain **O-b$_0$-b$_1$-q-O** and casting them in vector form as follows,

$$\boldsymbol{A}\begin{bmatrix}\delta\theta_3\\ \delta\boldsymbol{q}\end{bmatrix} = \boldsymbol{H_0}\begin{bmatrix}\delta v_{a_0}\\ \delta v_{b_0}\end{bmatrix} + \boldsymbol{H_{q\alpha}}\begin{bmatrix}\delta\alpha_a\\ \delta\alpha_b\end{bmatrix} + \boldsymbol{B}\begin{bmatrix}\delta v_{a_1}\\ \delta v_{b_1}\end{bmatrix} + \boldsymbol{H_q}\begin{bmatrix}\delta v_{q_a}\\ \delta v_{q_b}\end{bmatrix} + \boldsymbol{H_{q\beta}}\begin{bmatrix}\delta\beta_a\\ \delta\beta_b\end{bmatrix} \tag{7}$$

where

$$A = \begin{bmatrix} -v_{a_1}v_{q_a}\boldsymbol{u}_{\boldsymbol{a_1}}^{T_{q_a}} & v_{a_1}\boldsymbol{u}_{\boldsymbol{a_1}}^T \\ -v_{b_1}v_{q_b}\boldsymbol{u}_{\boldsymbol{b_1}}^{T_{q_b}} & v_{b_1}\boldsymbol{u}_{\boldsymbol{b_1}}^T \end{bmatrix}, \quad B = \begin{bmatrix} v_{a_1} & 0 \\ 0 & v_{b_1} \end{bmatrix} \tag{8}$$

$$\boldsymbol{H_0} = \mathrm{diag}\left[v_{a_1}\boldsymbol{u}_{\boldsymbol{a_1}}^T\boldsymbol{u}_{\boldsymbol{a}0} \quad v_{b_1}\boldsymbol{u}_{\boldsymbol{b_1}}^T\boldsymbol{u}_{b\,0}\right] \tag{9}$$

$$\boldsymbol{H_{q\alpha}} = \mathrm{diag}\left[v_{a_1}v_{a_0}\boldsymbol{u}_{\boldsymbol{a_1}}^T\boldsymbol{E}\boldsymbol{u}_{\boldsymbol{a}0} \quad v_{b_1}v_{b_0}\boldsymbol{u}_{\boldsymbol{b_1}}^T\boldsymbol{E}\boldsymbol{u}_{b\,0}\right] \tag{10}$$

$$\boldsymbol{H_q} = \mathrm{diag}\left[v_{a_1}\boldsymbol{u}_{\boldsymbol{a_1}}^{T_{q_a}} \quad v_{b_1}\boldsymbol{u}_{\boldsymbol{b_1}}^{T_{q_b}}\right] \tag{11}$$

$$\boldsymbol{H_{q\beta}} = \mathrm{diag}\left[v_{a_1}v_{q_a}\boldsymbol{u}_{\boldsymbol{a_1}}^{T_{q_a}} \quad v_{b_1}v_{q_b}\boldsymbol{u}_{\boldsymbol{b_1}}^{\boldsymbol{T}}\boldsymbol{E}\boldsymbol{u}_{\boldsymbol{q_b}}[]\right] \tag{12}$$

Matrix **A** is the direct matrix and **B** is the inverse Jacobian matrix of the mechanism. Suppose that **A** is a nonsingular matrix, i.e., the mechanism will not meet any Type II singularity [24]. The following is attained upon the multiplication of Eq. (7) by $\mathbf{A}^{-1}$:

$$\begin{bmatrix}\delta\theta_3\\ \delta\boldsymbol{q}\end{bmatrix} = \boldsymbol{J_0}\begin{bmatrix}\delta v_{a_0}\\ \delta v_{b_0}\end{bmatrix} + \boldsymbol{J_\alpha}\begin{bmatrix}\delta\alpha_a\\ \delta\alpha_b\end{bmatrix} + \boldsymbol{J}\begin{bmatrix}\delta v_{a_1}\\ \delta v_{b_1}\end{bmatrix} + \boldsymbol{J_q}\begin{bmatrix}\delta v_{q_a}\\ \delta v_{q_b}\end{bmatrix} + \boldsymbol{J_\beta}\begin{bmatrix}\delta\beta_a\\ \delta\beta_b\end{bmatrix} \tag{13}$$

with $\boldsymbol{J_0} = \boldsymbol{A^{-1}H_0}$, $\boldsymbol{J_{q\alpha}} = \boldsymbol{A^{-1}H_{q\alpha}}$, $\boldsymbol{J_q} = \boldsymbol{A^{-1}H_q}$, $\boldsymbol{J_{q\beta}} = \boldsymbol{A^{-1}H_{q\beta}}$, $\boldsymbol{J} = \boldsymbol{A^{-1}B}$. **J** is the kinematic Jacobian matrix of the mechanism and $\boldsymbol{J}_0, \boldsymbol{J_{q\alpha}}, \boldsymbol{J_q}$and $\boldsymbol{J_{q\beta}}$ are the sensitivity Jacobian matrices of the coupler pose.

The previous sensitivity analysis was for point **q** and should be applied for **p** and **r** points too using Eq. (14) and (15). The genetic algorithm will optimize the location of the pivots based on the sensitivity of the hood poses an error margin on the mechanism synthesis.

$$\begin{bmatrix}\delta\theta_3\\ \delta\boldsymbol{p}\end{bmatrix} = \boldsymbol{J_0}\begin{bmatrix}\delta v_{a_0}\\ \delta v_{b_0}\end{bmatrix} + \boldsymbol{J_{p\alpha}}\begin{bmatrix}\delta\alpha_a\\ \delta\alpha_b\end{bmatrix} + \boldsymbol{J}\begin{bmatrix}\delta v_{a_1}\\ \delta v_{b_1}\end{bmatrix} + \boldsymbol{J_p}\begin{bmatrix}\delta v_{p_a}\\ \delta v_{p_b}\end{bmatrix} + \boldsymbol{J_{p\beta}}\begin{bmatrix}\delta\beta_a\\ \delta\beta_b\end{bmatrix} \tag{14}$$

$$\begin{bmatrix}\delta\theta_3\\ \delta\boldsymbol{r}\end{bmatrix} = \boldsymbol{J_0}\begin{bmatrix}\delta v_{a_0}\\ \delta v_{b_0}\end{bmatrix} + \boldsymbol{J_{r\alpha}}\begin{bmatrix}\delta\alpha_a\\ \delta\alpha_b\end{bmatrix} + \boldsymbol{J}\begin{bmatrix}\delta v_{a_1}\\ \delta v_{b_1}\end{bmatrix} + \boldsymbol{J_r}\begin{bmatrix}\delta v_{r_a}\\ \delta v_{rb}\end{bmatrix} + \boldsymbol{J_{r\beta}}\begin{bmatrix}\delta\beta_a\\ \delta\beta_b\end{bmatrix} \tag{15}$$

GENETIC ALGORITHM

Likewise, in GA optimization, the problem parameters have to be frequently encoded into a string of either (1) binary bits, (2) real numbers or (3) characters. Parameters are recombined with selection crossover and mutation generation by generation until the fit solution is achieved within the problem search space.

Firstly, GA generates an initial population containing N chromosomes or individuals, each individual contains M genes that represent the problem variables or parameters. In this research, the variables are the mechanism moving and fixed pivots; so the chromosome has 8 real-valued genes (a_{0x}, a_{0y}, a_{1x}, a_{1y}, b_{0x}, b_{0y}, b_{1x}, b_{1y}). The values of the initial population's genes are chosen randomly from the predefined pivots' location ranges. GA selects the highly fitted chromosomes to carry their goodness to the next generation, the most common selection procedure is the Rolette Wheel selection. The fitness function is the sum of the errors in the constant length of links $\mathbf{a_0a_1}$ and $\mathbf{b_0b_1}$.

$$f(\boldsymbol{x}) = \sum_{i=2}^{N}\begin{Bmatrix}[([D_{1i}]\boldsymbol{a_1} - \boldsymbol{a_0})^T([D_{1i}]\boldsymbol{a_1} - \boldsymbol{a_0}) - (\boldsymbol{a_1} - \boldsymbol{a_0})^T(\boldsymbol{a_1} - \boldsymbol{a_0})]^2 \\ +[([D_{1i}]\boldsymbol{b_1} - \boldsymbol{b_0})^T([D_{1i}]\boldsymbol{b_1} - \boldsymbol{b_0}) - (\boldsymbol{b_1} - \boldsymbol{b_0})^T(\boldsymbol{b_1} - \boldsymbol{b_0})]^2\end{Bmatrix} \tag{16}$$

where $\boldsymbol{x} = \left(a_{0x}, a_{0y}, a_{1x}, a_{1x}, b_{0x}, b_{0x}, b_{1x}, b_{1x}\right)^T$

The next process is reproduction, which makes use of two operations: crossover and mutation. In the crossover operation, a certain percentage (crossover percentage; P_c) of the selected chromosomes (parents) are chosen to be recombined to give new chromosomes (children or offspring). The next step is the mutation operation, where an occasional deformation of a gene is occurred by a predefined mutation percentage over a generation's chromosomes. The new children will pass to the next generation, where the generation size is maintained.

Now, the selection, crossover and mutation operations are repeated. Until a termination criterion is finally met, usually to meet a specified number of generations. This approach produces successive generations with higher fitness to the data. Here are some main parameters considered in the GA method:

i. Fitness function: the function that measures each individual fit
ii. Population: Several individuals that GA method starts with, to obtain the next generations
iii. Selection: a process of choosing the fittest individuals from a population
iv. Crossover: a process that combines two parents to produce children for the next generation
v. Mutation: a process that applies random changes on parents to produce children.

EXAMPLE PROBLEM

In this study, the design of the vehicle hood was tested in various scenarios using MATLAB to ensure the generated four-bar will achieve various cases of locations. Equation (16) was used as a fitness function and Eq.s (13) to (15) as constraints in GA. Six cases will be discussed in this paper to demonstrate the sensitivity analysis of four-bar motion generation using GA. The results of this nonlinear analysis was then applied to design a car hood four-bar mechanism. The first four of six cases include seven poses for each quadrant. Case five includes 14 poses in one crank revolution and the last case includes 21 poses over full crank revolution. The following parameters are illustrated as an example for the first case (Seven poses in the first quadrant). Table 1 shows the parameters were used in the GA process.

Table 1. Parameters used in the GA process.

Characteristics	Items
Number of variables	8 (Mechanism joints' locations)
The population size	200
Number of generations	2000
Fitness value	0.001
Selection	SUS
The cross over fraction	0.8

Case I: Seven Poses First Quadrant

In this case, seven poses for the coupler points **p**, **q**, and **r** within the first quadrant were prescribed to study the motion of the four-bar mechanism. Initial guesses for the mechanism pivots were given as a_{0x}=[-0.5,0.5], a_{0y}=[-0.5,0.5], a_{1x} =[2,3.5], a_{1y} =[0,1.5], b_{0x} =[6.5,8], b_{0x} =[-0.5,0.5], b_{1x} =[8.5,10.5] and b_{1y} =[5.5,7]. The error constraints in coupler points **p**, **q**, and **r** as per Eq. (13) to (15) should not exceed 1/64 (0.015**)** inch. PS Shiakolas, et al. concluded that the synthesis is greatly affected by the quality of the initial guess [26]. This is true for Newton Raphson technique to solve the line search method through sequential quadratic programming. However, GA is an optimization process that is not affected by the quality of the initial guesses. Also, it is not limited to a certain number of poses like the Newton-Raphson technique. In the authors' work [27] eight prescribed coupler poses were prescribed. This is nearly twice the maximum number of prescribed displacements available with the conventional motion generation method described in [21].

The achieved optimal pivot locations are obtained using GA which are: $\mathbf{a_0}$= (0.2199,0.4994), $\mathbf{a_1}$= (2.8240, 1.3042), $\mathbf{b_0}$= (6.8733, -0.4500), and $\mathbf{b_1}$= (10.2630,6.5000) with fval= 0.001. Table 2 shows the mean absolute error (MAE), the difference in the crank angle and the MAE error of **p**, **q**, and **r** points for seven poses in the first quadrant. Table 3 shows the prescribed and achieved **p**, **q**, and **r** in the first quadrant.

Table 2. The MAE error and difference in the crank angle and the MAE error of p, q, and r coupler points for seven poses in the first quadrant.

Poses	Crank angle		**p**, **q**, and **r** coupler points		
	MAE Error	difference*	**p** MAE	**q** MAE	**r** MAE
1	0.0000	0.0000	0.0000	0.0000	0.0000
2	0.0024	10.8042	0.0025	0.0024	0.0024
3	0.0054	21.7810	0.0058	0.0058	0.0047
4	0.0052	32.7229	0.0057	0.0057	0.0043
5	0.0025	43.5858	0.0030	0.0026	0.0021
6	0.0021	54.3400	0.0029	0.0014	0.0019
7	0.0070	65.1059	0.0110	0.0068	0.0031

Table 3. The prescribed and achieved p, q, and r in the first quadrant.

Poses		p		q		r	
		Prescribed	Achieved	Prescribed	Achieved	Prescribed	Achieved
1	x	4.3171	4.3171	5.8151	5.8151	7.7396	7.7396
	y	3.0276	3.0276	5.0291	5.0291	5.5733	5.5733
2	x	4.2375	4.2415	5.8770	5.8811	7.8359	7.8401
	y	3.3874	3.3883	5.2748	5.2756	5.6778	5.6783
3	x	4.0295	4.0340	5.7608	5.7678	7.7374	7.7448
	y	3.7318	3.7388	5.5353	5.5400	5.8403	5.8423
4	x	3.7160	3.7181	5.5036	5.5085	7.4889	7.4941
	y	4.0458	4.0551	5.7935	5.8000	6.0357	6.0390
5	x	3.3186	3.3183	5.1372	5.1378	7.1265	7.1272
	y	4.3135	4.3191	6.0290	6.0336	6.2356	6.2391
6	x	2.8570	2.8583	4.6880	4.6865	6.6787	6.6768
	y	4.5213	4.5169	6.2235	6.2222	6.4158	6.4177
7	x	2.3499	2.3539	4.1789	4.1744	6.1694	6.1639
	y	4.6588	4.6407	6.3631	6.3540	6.5577	6.5584

Figure 4 shows the MAE (scalar) error of the corresponding 7 poses in the first quadrant, the MAE does not exceed 0.0110 for the three coupler points **p**, **q**, and **r**.

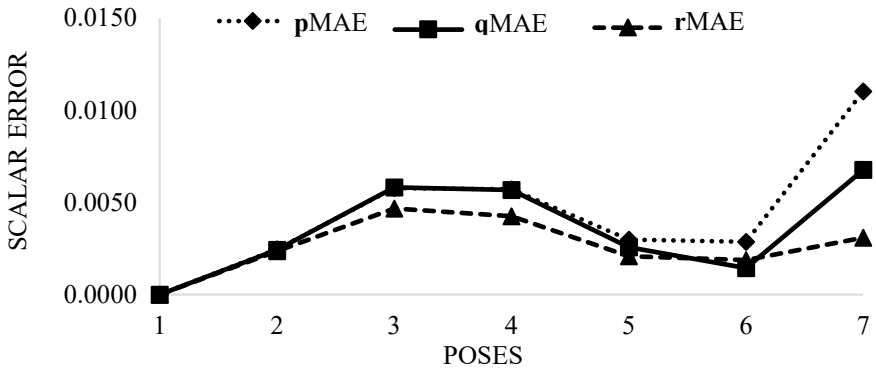

Figure. 4. Four-bar scalar error of the corresponding 7 poses in the first quadrant.

According to the author's previous work which was done on four-bar mechanism synthesis under elastic constraints using the Newton-Raphson analytical approach, GA is more powerful and accurate [10-12]. However, using appropriate GA parameters helps attain the optimal solution. For example, GA needs a sufficient number of population size (i.e. number of individuals) to increase the chances to reach the optimal solution over the prescribed gene boundaries. In addition, a sufficient number of generations increase the accuracy of the solution. GA starts its initial population with n size, 200 in our case, and then starts improving it by giving new generations with the same size. Three operations in GA are used; selection, crossover and mutation until a termination criterion is finally met. One of the GA stopping criterion used in this work it is to meet 2000 generations in order to produce successive generations with a higher fitted solution. The constraints Eq. (13) to (15) and goal function Eq. (16) were carried out at every function generation process in GA as illustrated in the flowchart of Figure 14.

The global optimum within 2000 generations for the pivots $\mathbf{a_0}$,$\mathbf{a_1}$,$\mathbf{b_0}$ and $\mathbf{b_1}$ is shown in Figure 6. It is vividly clear how the iterations (i.e. solutions) initially were widely spread over the initial given range and then coming together more condensed as approaching the allowable criterion. The motion of the coupler link is shown in Figure 5, where the achieved **p**, **q**, and **r** coupler points are almost equal to the prescribed ones in seven poses.

GA always looks for the fittest solution as illustrated in Figure 6. The optimal synthesized four-bar pivot locations; (a) (a_{0x}, a_{0y}) ,(b) (a_{1x}, a_{1y}), (c) (b_{0x},b_{0y}), and (d) (b_{1x}, b_{1y}) were chosen from a large set of population. Also, in Figure 6, the clustering of the solution points in one place shows first, the solution is converging to the clustering region. Second, building confidence in the sought solution, especially when approaching global minimum within the specified interval.

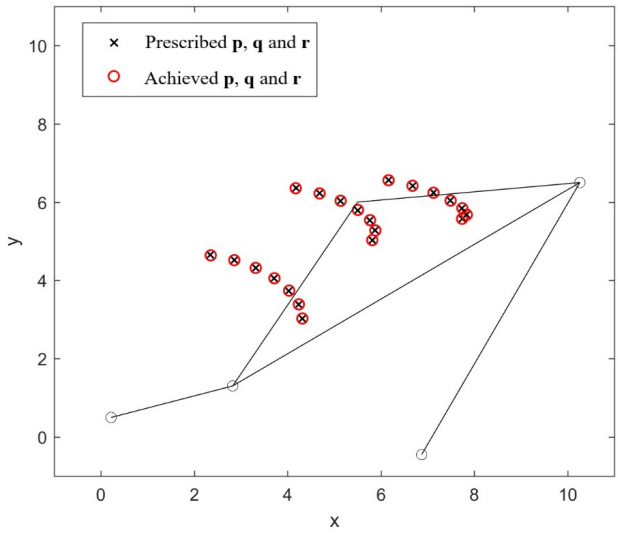

Figure 5. Schematic diagram shows prescribed and achieved poses of the coupler curve in the first quadrant.

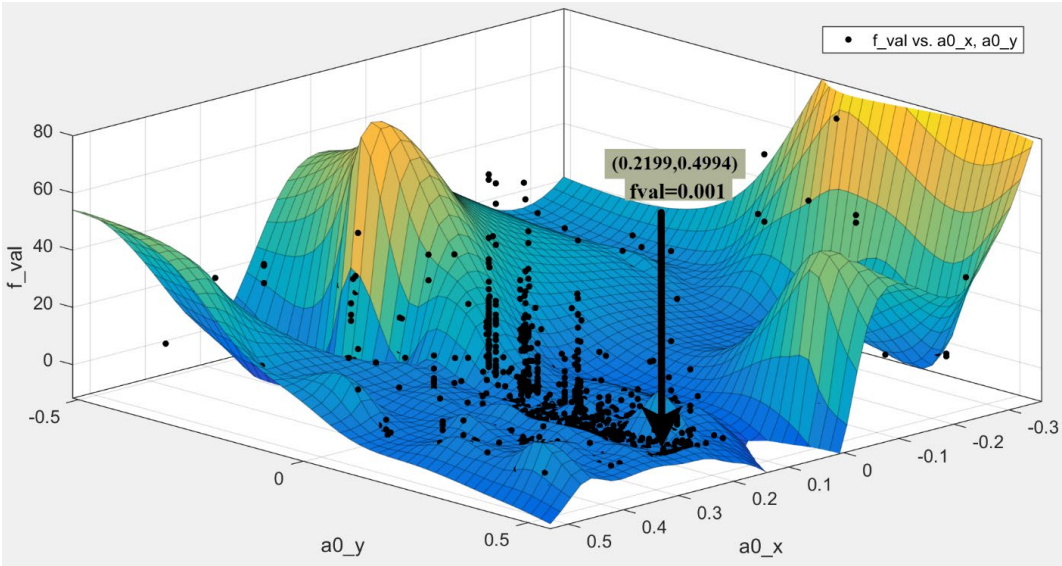

(a) (a_{0x}, a_{0y})

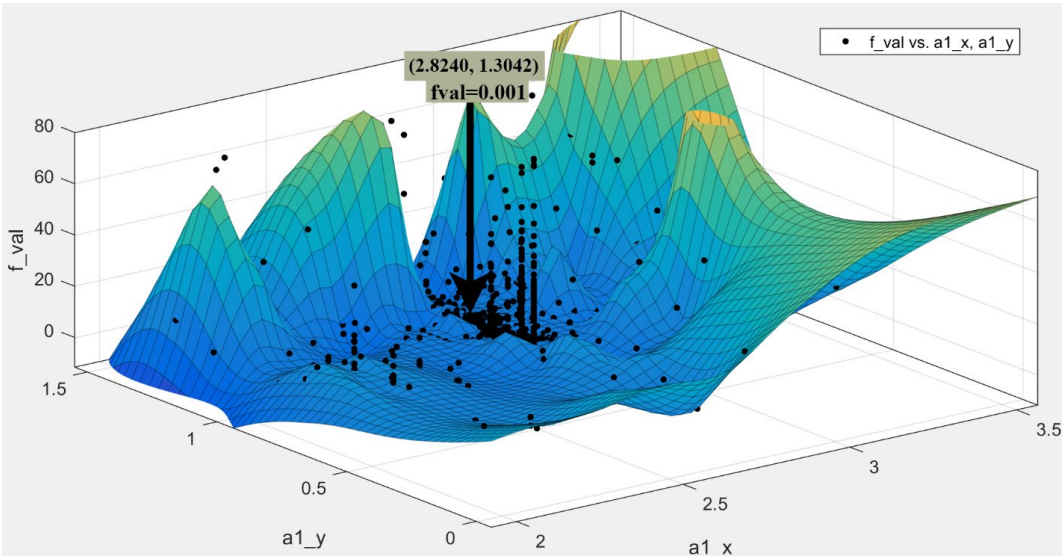

(b) (a_{1x}, a_{1y})

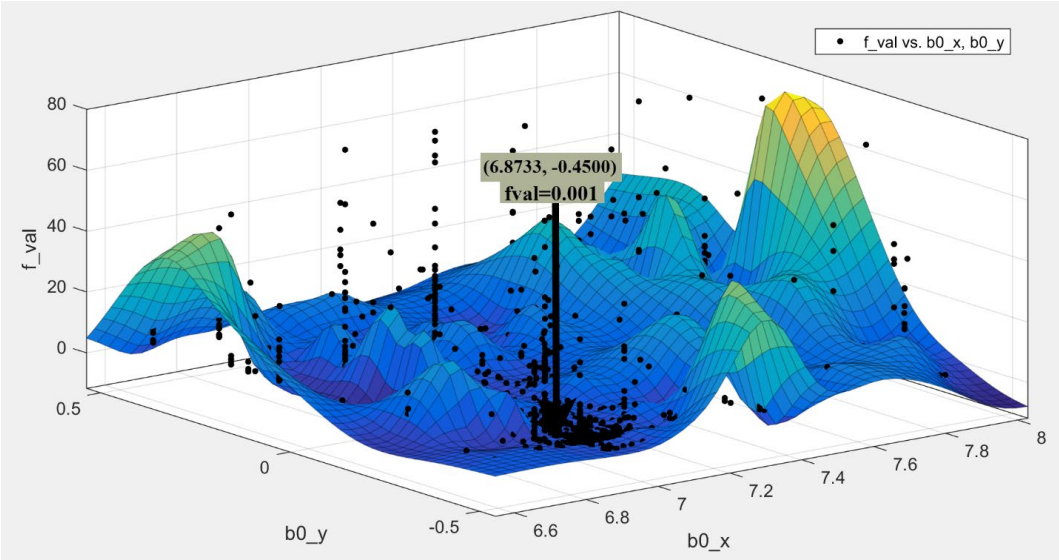

(c) (b_{0x},b_{0y})

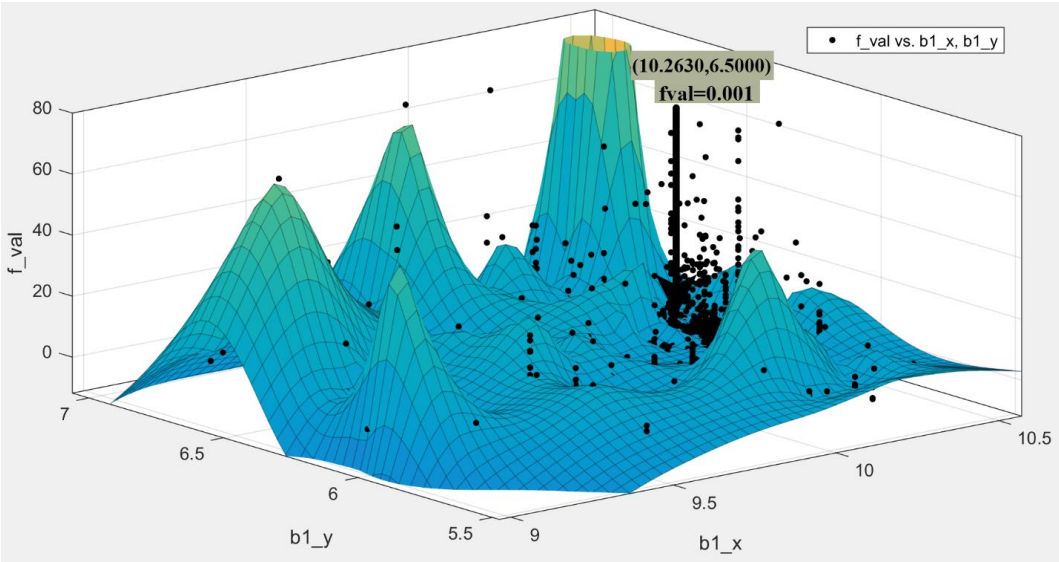

(d) (b_{1x}, b_{1y})

Figure 6. Zoom-in view for the optimal synthesized four-bar pivot locations.

Case II: Seven Poses Second Quadrant

The work performed for Case I was then projected on other quadrants as shown in cases II to IV. Angeles studied the invariants of an orthogonal matrix for the first two quadrants because the sign change of crank rotation angle [28] as shown in Eq. (17). Since the crank is rotating in all four quadrants, it is expected that the sign changes. Hence, the rotation matrix. The trace matrix Q has to be either 3 or -1 to be symmetric and hence be a rotation matrix.

$$\mathbf{Q} = \mathbf{e}\mathbf{e}^{\mathrm{T}}+\cos\theta(\mathbf{I}-\mathbf{e}\mathbf{e}^{\mathrm{T}})+\sin\theta\mathbf{E} \tag{17}$$

$$\mathrm{tr}(\mathbf{Q}) = \mathrm{tr}(\mathbf{e}\mathbf{e}^{\mathrm{T}})+ \mathrm{tr}[\cos\theta(\mathbf{I}-\mathbf{e}\mathbf{e}^{\mathrm{T}})]+ \mathrm{tr}(\sin\theta\mathbf{E}) \tag{18}$$

$$\mathrm{tr}(\mathbf{Q}) = 1+2\cos\theta \tag{19}$$

tr(**Q**) depends on which quadrant θ lies in. Where **Q**, **ee**, **I**, θ and **E** are rotation orthogonal matrix, symmetric, rank-one matrix, crank rotation angle, and cross-product matrix of the unit vector **e**, respectively.

This work expands beyond two first quadrants to study all quadrants and full rotation for the crank angle as shown in Cases V and IV. In case II, the crank rotates within the second quadrant, the optimal joints' locations are obtained using GA which are: $\mathbf{a_0}$= (0.3455, 0.2286), $\mathbf{a_1}$=(0.0000, 3.4993), $\mathbf{b_0}$= (6.6587, 0.5000), and $\mathbf{b_1}$= (7.4471, 6.1737) with fval= 0.001. The solution depends on seven desired poses in the second quadrant. Table 4 shows the MEA error and difference in the crank angle and the MEA error of **p**, **q**, and **r** coupler points for seven poses in the second quadrant. Table 5 shows the prescribed and achieved **p**, **q**, and **r** in the second quadrant

Table 4. The MAE error and difference in the crank angle and the MAE error of **p**, **q**, and **r** coupler points for seven poses in the second quadrant.

	Crank angle		**p**, **q**, and **r** couple points		
Poses	MAE error	difference	**p** MAE	**q** MAE	**r** MAE
1	0.0000	0.0000	0.0000	0.0000	0.0000
2	0.0041	13.7519	0.0066	0.0008	0.0050
3	0.0055	27.6343	0.0098	0.0014	0.0052
4	0.0051	41.5106	0.0104	0.0029	0.0020
5	0.0030	59.8391	0.0040	0.0029	0.0021
6	0.0021	68.8731	0.0040	0.0008	0.0017
7	0.0053	73.3631	0.0094	0.0038	0.0026

Table 5. The prescribed and achieved **p**, **q**, and **r** in the second quadrant.

Poses		**p**		**q**		**r**	
		Prescribed	Achieved	Prescribed	Achieved	Prescribed	Achieved
1	x	1.5428	1.5428	3.3470	3.3470	5.3345	5.3345
	y	4.7191	4.7191	6.4497	6.4497	6.6729	6.6729
2	x	0.7306	0.7366	2.4874	2.4861	4.4681	4.4657
	y	4.5978	4.5906	6.3766	6.3764	6.6536	6.6612
3	x	-0.0333	-0.0245	1.6541	1.6535	3.6228	3.6203
	y	4.3021	4.2913	6.1467	6.1446	6.4992	6.5070
4	x	-0.7025	-0.6927	0.8932	0.8949	2.8424	2.8423
	y	3.8529	3.8420	5.7774	5.7732	6.2253	6.2292
5	x	-1.3833	-1.3790	0.0525	0.0439	1.9594	1.9621
	y	3.0726	3.0689	5.1192	5.1241	5.7223	5.7207
6	x	-1.6155	-1.6200	-0.2766	-0.2771	1.6002	1.6010
	y	2.6322	2.6358	4.7434	4.7445	5.4346	5.4321
7	x	-1.7024	-1.7139	-0.4162	-0.4208	1.4428	1.4406
	y	2.4052	2.4125	4.5490	4.5521	5.2865	5.2835

Figure 7 shows the scalar error of the corresponding 7 poses in the second quadrant, the MAE does not exceed 0.0104 for the three coupler points **p**, **q**, and **r**

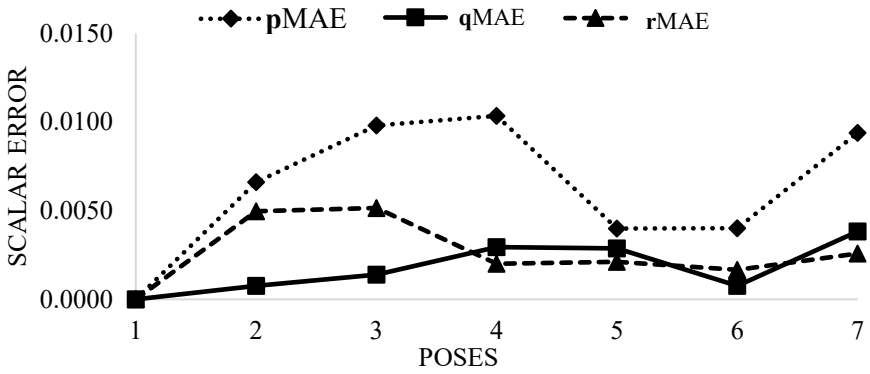

Figure 7. Four-bar scalar error for the corresponding 7 poses in the second quadrant.

Case III: Seven Poses Third Quadrant

In this case, the crank link rotates within the third quadrant. The optimal joints' locations are obtained using GA which are: $\mathbf{a}_0$= (0.3635, 0.3653), $\mathbf{a}_1$= (-2.0008, 0.3444), $\mathbf{b}_0$= (7.2016, -0.0810), and $\mathbf{b}_1$= (3.1787, 6.4975) with fval= 0.001. The solution depends on seven desired poses in the third quadrant. Table 6 shows the MEA error and difference in the crank angle and the MEA error of **p**, **q**, and **r** points for seven poses in the third quadrant. Table 7 shows the prescribed and achieved **p**, **q**, and **r**, the third quadrant.

Table 6. The MEA error and difference in the crank angle and the MEA error of **p**, **q**, and **r** points for seven poses in the third quadrant.

Poses	Crank Angle		**p, q**, and **r** couple points		
	MAE Error	difference	p MAE	q MAE	r MAE
1	0.0000	0.0000	0.0000	0.0000	0.0000
2	0.0022	16.7905	0.0033	0.0009	0.0023
3	0.0031	33.3781	0.0033	0.0011	0.0047
4	0.0038	49.8522	0.0043	0.0017	0.0053
5	0.0044	66.4897	0.0055	0.0036	0.0040
6	0.0016	83.6550	0.0028	0.0016	0.0005
7	0.0078	95.0632	0.0069	0.0077	0.0086

Table 7. The prescribed and achieved **p**, **q**, and **r** in the third quadrant.

Poses		**p**		**q**		**r**	
		Prescribed	Achieved	Prescribed	Achieved	Prescribed	Achieved
1	x	-1.8163	-1.8163	-0.6440	-0.6440	1.1739	1.1739
	y	1.9466	1.9466	4.1548	4.1548	4.9886	4.9886
2	x	-1.8374	-1.8429	-0.8557	-0.8569	0.8853	0.8860
	y	1.2731	1.2742	3.5723	3.5716	4.5566	4.5527
3	x	-1.6857	-1.6921	-0.9140	-0.9141	0.7318	0.7347
	y	0.6572	0.6570	3.0351	3.0329	4.1714	4.1649
4	x	-1.3780	-1.3851	-0.8276	-0.8279	0.7071	0.7104
	y	0.1405	0.1390	2.5792	2.5762	3.8617	3.8543
5	x	-0.9384	-0.9447	-0.6089	-0.6110	0.8046	0.8049
	y	-0.2407	-0.2454	2.2375	2.2323	3.6524	3.6448
6	x	-0.3962	-0.3928	-0.2715	-0.2704	1.0209	1.0207
	y	-0.4575	-0.4597	2.0394	2.0374	3.5657	3.5648
7	x	0.0069	0.0062	0.0139	0.0116	1.2330	1.2297
	y	-0.5000	-0.4869	2.0000	2.0131	3.5855	3.5994

Figure 8 shows the scalar error of the corresponding 7 poses in the third quadrant, the MAE does not exceed 0.0086 for the three coupler points **p**, **q**, and **r**.

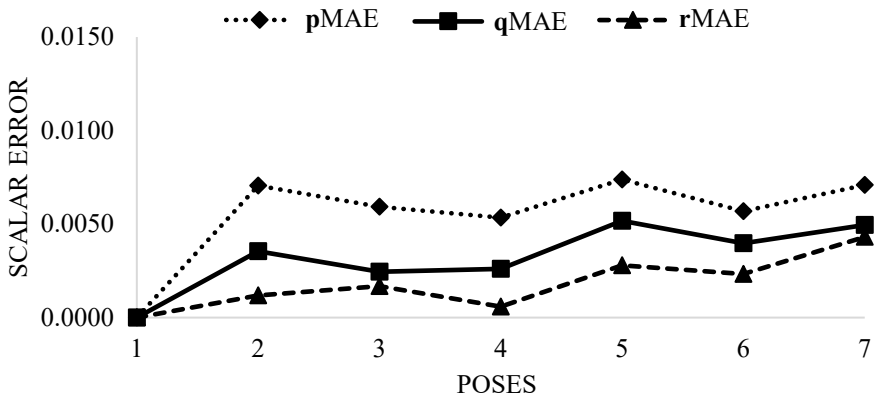

Figure 7. Four-bar scalar error for the corresponding 7 poses in the third quadrant.

Case IV: Seven Poses Fourth Quadrant

In this case, the crank link rotates within the fourth quadrant, the optimal joints' locations are obtained using GA which are: $\mathbf{a}_0$= (-0.824, -0.2663), $\mathbf{a}_1$= (-0.1671, -3.1287), $\mathbf{b}_0$= (7.0026,-0.1921), and $\mathbf{b}_1$= (2.7800, 5.3183). The solution depends on seven desired poses in the fourth quadrant. Table 8 shows the MEA error and difference in the crank angle and the MEA error of **p**, **q**, and **r** points for seven poses in the fourth quadrant. Table 9 shows the prescribed and achieved **p**, **q**, and **r**, in the fourth quadrant.

Table 8. The MEA error and difference in the crank angle and the MEA error of **p**, **q**, and **r** coupler points for seven poses in the fourth quadrant.

Poses	Crank angle		**p**, **q**, and **r** couple points		
	MAE Error	difference	**p** MAE	**q** MAE	**r** MAE
1	0.0000	0.0000	0.0000	0.0000	0.0000
2	0.0039	16.1930	0.0071	0.0036	0.0012
3	0.0034	31.9582	0.0059	0.0025	0.0017
4	0.0028	47.6018	0.0053	0.0026	0.0006
5	0.0051	63.3842	0.0074	0.0052	0.0028
6	0.0040	79.5066	0.0057	0.0040	0.0023
7	0.0055	90.7707	0.0071	0.0050	0.0043

Table 9. The prescribed and achieved **p**, **q**, and **r** in the fourth quadrant.

Poses		**p**		**q**		**r**	
		Prescribed	Achieved	Prescribed	Achieved	Prescribed	Achieved
1	x	0.0069	0.0069	0.0139	0.0139	1.2330	1.2330
	y	-0.5000	-0.5000	2.0000	2.0000	3.5855	3.5855
2	x	0.6531	0.6635	0.5298	0.5329	1.6646	1.6629
	y	-0.4008	-0.4045	2.0961	2.0921	3.7430	3.7423
3	x	1.3300	1.3404	1.1601	1.1630	2.2639	2.2618
	y	-0.1039	-0.1053	2.3904	2.3884	4.0582	4.0595
4	x	2.0276	2.0362	1.9339	1.9367	3.0881	3.0872
	y	0.3769	0.3748	2.8752	2.8728	4.5085	4.5088
5	x	2.7439	2.7541	2.8898	2.8957	4.1951	4.1985
	y	0.9957	0.9911	3.4915	3.4871	5.0068	5.0046
6	x	3.4488	3.4558	3.9998	4.0040	5.5348	5.5375
	y	1.6621	1.6577	4.1006	4.0969	5.3827	5.3808
7	x	3.8567	3.8533	4.7248	4.7245	6.4156	6.4168
	y	2.0830	2.0938	4.4274	4.4371	5.4956	5.5030

Figure9 shows the scalar error of the corresponding 7 poses in the fourth quadrant, the MAE does not exceed 0.0074 for the three coupler points **p**, **q**, and **r**.

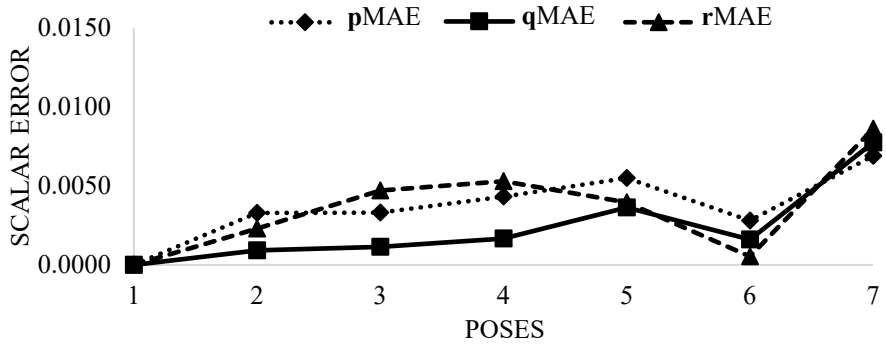

Figure 9. Four-bar scalar error for the corresponding 7 poses in the fourth quadrant.

Case V: Fourteen Poses over 360 Degree

In this case, the crank link rotates within 360°. The optimal joints' locations are obtained using GA which are: $\mathbf{a}_0$= (0.0828, 0.732), $\mathbf{a}_1$= (2.9143, 1.0509), $\mathbf{b}_0$= (6.9656, -0.1690), and $\mathbf{b}_1$= (10.0947, 6.2921), with fval= 0.0700. The error constraints in coupler points **p**, **q**, and **r** as per Eq. (13) to (15) should not exceed 1/16 (0.0625) inch in cases V and VI. The solution depends on 14 desired poses in 360°. Table 10 shows MEA error and difference in the crank angle and the MEA error of **p**, **q**, and **r** coupler points for 14 poses in 360°. Table 11 shows the prescribed and achieved **p**, **q**, and **r** in 360°.

Table 10. The MEA error and difference in the crank angle and the MEA error of **p**, **q**, and **r** coupler points for 14 poses in full crank rotation 360°.

Poses	Crank angle		**p**, **q**, and **r** couple points		
	MAE Error	difference	**p** MAE	**q** MAE	**r** MAE
1	0.0000	0.0000	0.0000	0.0000	0.0000
2	0.0230	25.4843	0.0216	0.0216	0.0259
3	0.0175	51.1538	0.0254	0.0180	0.0090
4	0.0138	81.3960	0.0266	0.0087	0.0062
5	0.0105	106.4633	0.0204	0.0042	0.0067
6	0.0064	131.5751	0.0121	0.0019	0.0052
7	0.0022	156.6143	0.0026	0.0008	0.0033
8	0.0035	181.6022	0.0053	0.0026	0.0026
9	0.0073	211.3577	0.0096	0.0059	0.0063
10	0.0066	236.0736	0.0080	0.0026	0.0092
11	0.0061	261.0257	0.0070	0.0026	0.0088
12	0.0053	286.0512	0.0085	0.0021	0.0054
13	0.0026	310.8704	0.0044	0.0024	0.0011
14	0.0013	330.6508	0.0019	0.0005	0.0016

Table 11. The prescribed and achieved **p**, **q**, and **r** in full crank rotation 360°.

Poses		**p**		**q**		**r**	
		Prescribed	Achieved	Prescribed	Achieved	Prescribed	Achieved
1	x	4.3171	4.3171	5.8151	5.8151	7.7396	7.7396
	y	3.0276	3.0276	5.0291	5.0291	5.5733	5.5733
2	x	3.8845	3.8650	5.6477	5.6311	7.6294	7.6105
	y	3.8937	3.8700	5.9666	5.9400	5.9357	5.9686
3	x	2.8570	2.8505	4.6880	4.7019	6.6787	6.6947
	y	4.5213	4.5656	6.2235	6.2456	6.4158	6.4138
4	x	1.2699	1.2523	3.0607	3.0629	5.0464	5.0512
	y	4.6988	4.7345	6.4432	6.4583	6.6818	6.6742
5	x	-0.0333	-0.0501	1.6541	1.6543	3.6228	3.6262
	y	4.3021	4.3261	6.1467	6.1550	6.4992	6.4892
6	x	-1.0768	-1.0904	0.4445	0.4424	2.3753	2.3761
	y	3.4839	3.4945	5.4677	5.4695	5.9894	5.9799
7	x	-1.7024	-1.7060	-0.4162	-0.4156	1.4428	1.4448
	y	2.4052	2.4068	4.5490	4.5480	5.2865	5.2819
8	x	-1.8374	-1.8290	-0.8557	-0.8511	0.8853	0.8883
	y	1.2731	1.2708	3.5723	3.5716	4.5566	4.5588
9	x	-1.3780	-1.3621	-0.8276	-0.8213	0.7071	0.7084
	y	0.1405	0.1439	2.5792	2.5847	3.8617	3.8731
10	x	-0.5864	-0.5747	-0.3964	-0.3964	0.9356	0.9286
	y	-0.4050	-0.4006	2.0878	2.0930	3.5797	3.5912
11	x	0.4335	0.4459	0.3460	0.3431	1.5043	1.4915
	y	-0.4560	-0.4576	2.0425	2.0403	3.6729	3.6777
12	x	1.5604	1.5753	1.4000	1.4013	2.5103	2.5025
	y	0.0374	0.0353	2.5322	2.5293	4.1958	4.1988
13	x	2.7439	2.7514	2.8898	2.8935	4.1951	4.1966
	y	0.9957	0.9944	3.4915	3.4904	5.0068	5.0076
14	x	3.6633	3.6610	4.3721	4.3726	5.9874	5.9893
	y	1.8765	1.8779	4.2739	4.2745	5.4531	5.4519

Figure 10 shows the scalar error of the corresponding 14 poses in 360°, the MAE does not exceed 0.0266 for the three **p**, **q**, and **r**.

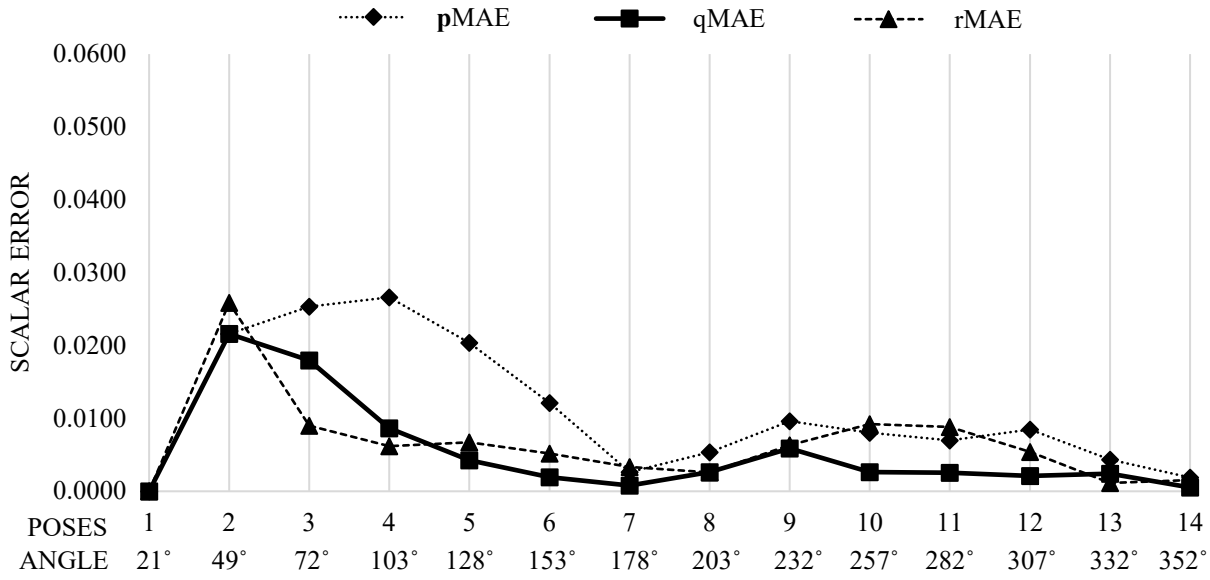

Figure 10. Four-bar scalar error for the corresponding 14 poses in 360°.

Case VI: Twenty-one Poses over 360 Degree

In this case, the crank link rotates within 360˚. The optimal joints' locations are obtained using GA which are: $\mathbf{a_0}$= (0.2624, 0.0977), $\mathbf{a_1}$= (3.0660, 1.0404) $\mathbf{b_0}$= (6.9385,-0.2959), and $\mathbf{b_1}$= (10.1766, 6.9436), with fval=0.0680. The solution depends on 21 desired poses in 360°. Table 12 shows the MEA error and difference in the crank angle and the MEA error of **p**, **q**, and **r** coupler points for 21 poses in 360°. Table 13 shows the prescribed and achieved **p**, **q**, and **r** in full crank rotation 360. Figure 11 shows the scalar error of the corresponding 21 poses in full crank rotation 360 degree, the MAE does not exceed 0.0459 for the three coupler points **p**, **q**, and **r**.

Table 12. The MEA error and difference in the crank angle and the MEA error of **p**, **q**, and **r** coupler points for 21 poses in full crank rotation 360˚.

Poses	Crank angle		**p**, **q**, and **r** points		
	MAE Error	difference	**p** MAE	**q** MAE	**r** MAE
1	0.0000	0.0000	0.0000	0.0000	0.0000
2	0.0336	15.8758	0.0318	0.0327	0.0363
3	0.0343	37.2885	0.0410	0.0356	0.0262
4	0.0299	52.6537	0.0459	0.0251	0.0189
5	0.0221	72.8178	0.0384	0.0135	0.0146
6	0.0159	87.8831	0.0292	0.0076	0.0110
7	0.0096	102.9553	0.0190	0.0040	0.0057
8	0.0026	123.0039	0.0037	0.0025	0.0017
9	0.0057	138.0748	0.0082	0.0015	0.0075
10	0.0128	158.0465	0.0231	0.0029	0.0125
11	0.0179	173.0021	0.0328	0.0068	0.0141
12	0.0204	187.6835	0.0345	0.0107	0.0161
13	0.0228	206.9689	0.0309	0.0176	0.0199
14	0.0198	221.2362	0.0254	0.0139	0.0201
15	0.0113	240.8268	0.0124	0.0060	0.0156
16	0.0207	256.2336	0.0294	0.0149	0.0178
17	0.0268	271.7417	0.0410	0.0233	0.0162
18	0.0223	291.9719	0.0366	0.0222	0.0080
19	0.0144	306.8748	0.0240	0.0147	0.0046
20	0.0023	326.5483	0.0024	0.0022	0.0022
21	0.0044	331.4756	0.0051	0.0042	0.0039

Table 13. The prescribed and achieved **p**, **q**, and **r** in crank full rotation 360°.

Poses		**p**		**q**		**r**	
		Prescribed	Achieved	Prescribed	Achieved	Prescribed	Achieved
1	x	4.3171	4.3171	5.8151	5.8151	7.7396	7.7396
	y	3.0276	3.0276	5.0291	5.0291	5.5733	5.5733
2	x	4.1481	4.1723	5.8387	5.8904	7.8080	7.8647
	y	3.5624	3.6017	5.4041	5.4178	5.7531	5.7373
3	x	3.5265	3.5225	5.3323	5.3684	7.3200	7.3607
	y	4.1864	4.2644	5.9153	5.9504	6.1368	6.1251
4	x	2.8570	2.8382	4.6880	4.7073	6.6787	6.7019
	y	4.5213	4.5942	6.2235	6.2543	6.4158	6.4013
5	x	1.8151	1.7914	3.6303	3.6381	5.6191	5.6305
	y	4.7191	4.7722	6.4382	6.4574	6.6489	6.6311
6	x	0.9985	0.9772	2.7735	2.7765	4.7570	4.7634
	y	4.6583	4.6954	6.4188	6.4310	6.6754	6.6598
7	x	0.2130	0.1966	1.9259	1.9249	3.8993	3.9010
	y	4.4190	4.4406	6.2399	6.2470	6.5650	6.5552
8	x	-0.7025	-0.7057	0.8932	0.8913	2.8424	2.8408
	y	3.8529	3.8571	5.7774	5.7806	6.2253	6.2271
9	x	-1.2390	-1.2308	0.2410	0.2385	2.1606	2.1551
	y	3.2827	3.2745	5.2976	5.2971	5.8591	5.8687
10	x	-1.7024	-1.6733	-0.4162	-0.4125	1.4428	1.4376
	y	2.4052	2.3881	4.549	4.5469	5.2865	5.3063
11	x	-1.8432	-1.7983	-0.7319	-0.7221	1.0624	1.0583
	y	1.7185	1.6977	3.9580	3.9542	4.8413	4.8653
12	x	-1.8054	-1.7483	-0.8919	-0.8735	0.8194	0.8203
	y	1.0593	1.0475	3.3864	3.3895	4.4215	4.4529
13	x	-1.4965	-1.4408	-0.8717	-0.8513	0.7015	0.7038
	y	0.2993	0.3053	2.7200	2.7348	3.9549	3.9924
14	x	-1.0978	-1.0608	-0.6956	-0.6861	0.7589	0.7530
	y	-0.1306	-0.1167	2.3368	2.3550	3.7096	3.7439
15	x	-0.3962	-0.3775	-0.2715	-0.2785	1.0209	0.9981
	y	-0.4575	-0.4635	2.0394	2.0345	3.5657	3.5740
16	x	0.2178	0.2495	0.1741	0.1724	1.3608	1.3374
	y	-0.4890	-0.5161	2.0107	1.9827	3.6205	3.6083
17	x	0.8761	0.9254	0.7262	0.7376	1.8434	1.8295
	y	-0.3236	-0.3562	2.1719	2.1367	3.8308	3.8123
18	x	1.7929	1.8412	1.6574	1.6750	2.7842	2.7813
	y	0.1982	0.1732	2.6945	2.6677	4.3469	4.3338
19	x	2.5036	2.5359	2.5498	2.5639	3.7936	3.7963
	y	0.7788	0.7632	3.2784	3.2630	4.8446	4.8382
20	x	3.4488	3.4521	3.9998	4.0026	5.5348	5.5373
	y	1.6621	1.6636	4.1006	4.1022	5.3827	5.3846
21	x	3.6633	3.6613	4.3721	4.3734	5.9874	5.9903
	y	1.8765	1.8846	4.2739	4.2811	5.4531	5.4581

Case I was performed to simulate the car hood opening in the rear-hinge like Figure 12(a) which is the first quadrant. Case II was performed to simulate the front-hinged hood opening or flipfront hinge like Figure 12(b) and 12(c). Other cases were performed as an expansion to the method and to represent other mechanisms where the crank rotates quadratically or in full rotation. This motion might represent the opening of the dutch lift bridge linkage or stamping mechanism where it covers three quadrants together like case III. Cases IV to VI were performed to test this probabilistic optimization technique. Cases V and Case VI can represent.

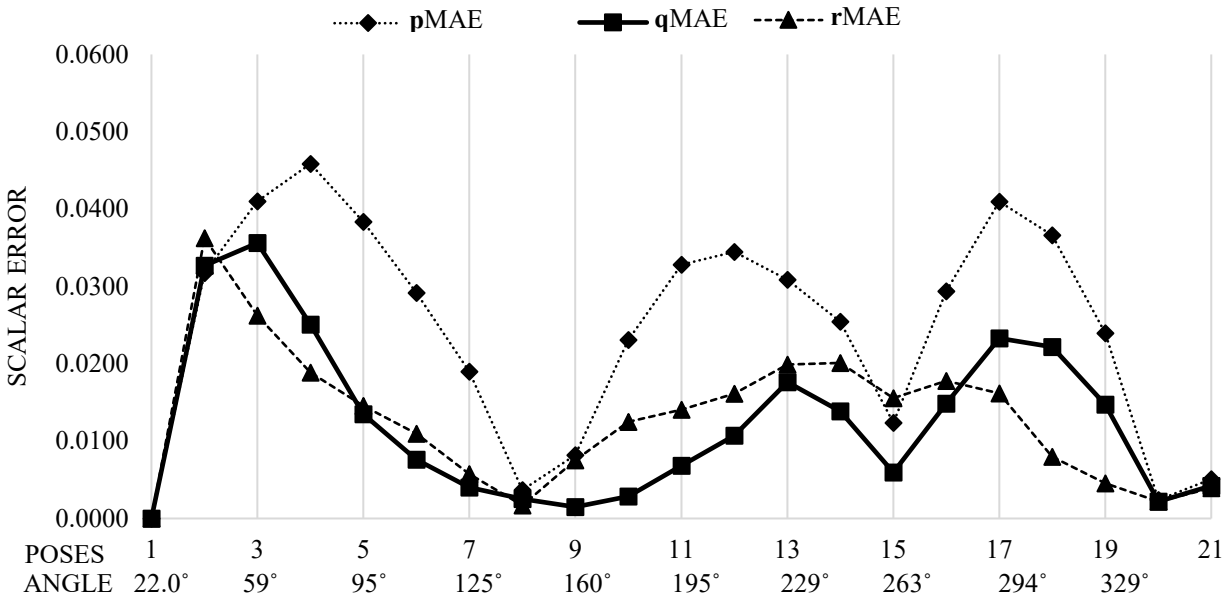

Figure 11. Four-bar scalar error for the corresponding 21 poses in 360 degree.

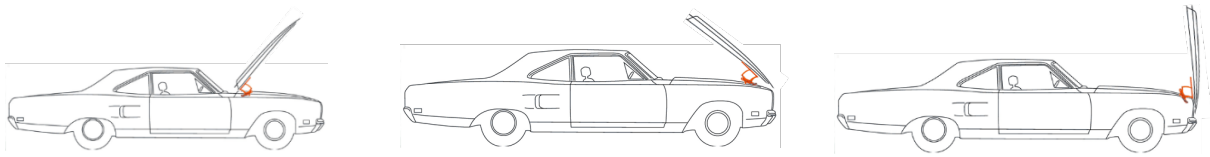

Figure 12. Schematic diagram for hood opening.

CONCLUSION

This paper presented an application of vehicle hood where the hood and the automobile body are linked with four-bar linkages. The working envelop of the hood must be fitted within the allotted space; therefore, its motion must undergo a specific motion or pose sequence. The nonlinear optimization problem presented in this work considers the sensitivity analysis and count for the error of the coupler (i.e. the hood) points **p**, **q**, and **r**. Equation (16) becomes invalid when the pivots $\mathbf{a}_1$, and $\mathbf{b}_1$ are collinear. Such a state is possible when the four-bar mechanism reaches a "lock-up" or binding position. The genetic algorithm was performed considering the sensitivity constraint of the hood poses on the mechanism synthesis according to the flowchart illustration Figure 14. The fitness function of the sum of the errors in the constant length of links $\mathbf{a}_0\mathbf{a}_1$ and $\mathbf{b}_0\mathbf{b}_1$ was checked for every generation. The results demonstrated that GA can synthesize the mechanism in various cases with minimum error. The results of this mechanism synthesis were utilized to manufacture the four-bar hood mechanism. A real example using the discussed nonlinear optimization synthesis is presented for the hood used in Plymouth Satellite automobile as shown in Figure 13. The mathematical analysis software MATLAB was used to codify and solve the formulated nonlinear optimization problem.

The expansion of application of the presented technique would help the designer to synthesize a four-bar mechanism with very satisfying and accurate levels. Four-bar mechanism applications such stamping mechanism described in author's work [29] runs between 0° and 180°. More sophisticated application such as artificial knee can utilize this technique for finding mechanism pivot coordinates with high accuracy. The results achieved by sensitivity constraints within the GA are more accurate and robust even for complex problems.

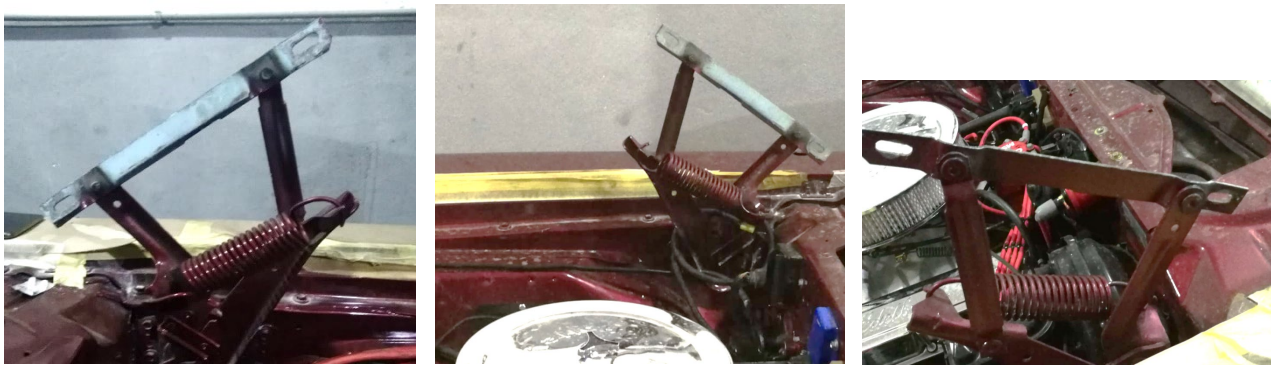

Figure 13. A real example of a GA designed hood four-bar mechanism used in Plymouth Satellite automobile.

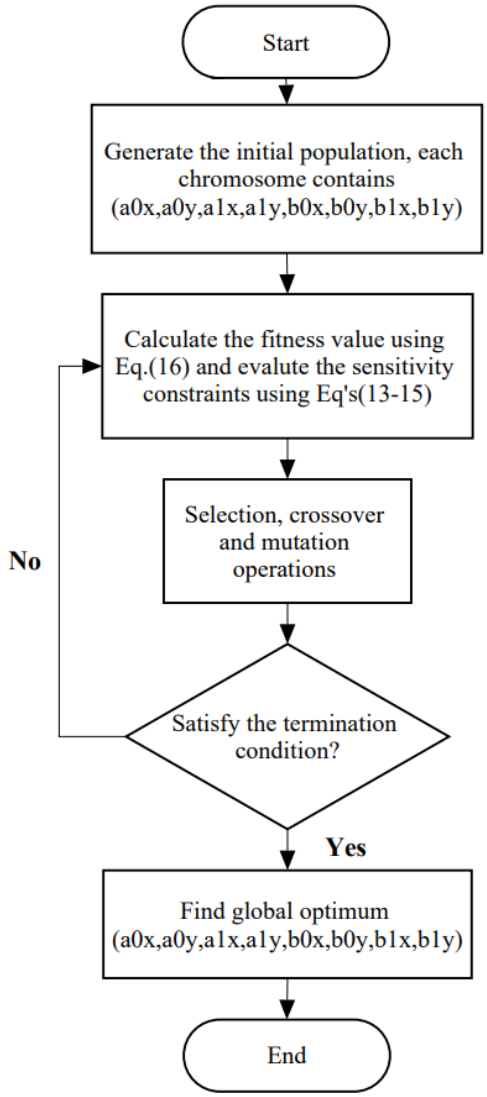

Figure 14. GA process flowchart.

REFERENCES

[1] S. Crocesi, and E. Pennestrì, "Kinematic synthesis of a curve-scribing mechanism for prescribed finite motion," *Mech. Mach. Theory*, vol. 40, no. 1, pp. 91–98, 2005,doi: 10.1016/j.mechmachtheory.2004.06.002.

[2] O. Denizhan, and M.-S. Chew, "Linkage mechanism optimization and sensitivity analysis of an automotive engine hood," *Int. J. Automot. Technol.*, vol. 1, no. 1, pp. 7–16, 2018,doi: 10.30939/ijastech..364438.

[3] S. Idlani, D.A. Streit, and B.J. Gilmore, "Elastic potential synthesis—a generalized procedure for dynamic synthesis of machine and mechanism systems," *J. Mech. Des.*, vol. 115, no. 3, pp. 568–575, 1993, doi: 10.1115/1.2919227.

[4] O.S. Ko, and C.H. Yu, "The opening mechanism analysis on hood, tail gate, and trunk lid by mathematical modeling," *SAE Technical Paper Series*, 1995, doi: 10.4271/950827.

[5] C.D. Untaroiu, J. Shin, and J.R. Crandall, "A design optimization approach of vehicle hood for pedestrian protection," *Int. J. Crashworthiness*, vol. 12, no. 6, pp. 581–589, 2007,doi: 10.1080/13588260701492947.

[6] K. Russell, Q. Shen, and R. S. Sodhi, 2013. *Mechanisms Design: Visual and Programmable Approaches*. Bosa Roca:: Taylor & Francis Inc, 2013.

[7] S.B. Matekar, and G.R. Gogate, "Optimum synthesis of path generating four-bar mechanisms using differential evolution and a modified error function," *Mech. Mach. Theory*, vol. 52, pp. 158–179, 2012,doi: 10.1016/j.mechmachtheory.2012.01.017.

[8] M.S. Osman, M.A. Abo-Sinna, and A.A. Mousa, "A combined genetic algorithm-fuzzy logic controller (GA–FLC) in nonlinear programming," *Appl. Math. Comput.*, vol. 170, no. 2, pp. 821–840, 2005,doi: 10.1016/j.amc.2004.12.023.

[9] N. Diab, and A. Smaili, "Optimum exact/approximate point synthesis of planar mechanisms," *Mech. Mach. Theory*, vol. 43, no. 12, pp.1610–1624, 2008, doi: 10.1016/j.mechmachtheory.2007.12.006.

[10] Y.M. Al-Smadi, Q. Shen, K. Russell, and R.S. Sodhi, "Planar four-bar motion generation with prescribed static torque and rigid-body reaction force," *Mech. Based Des. Struct. Mach.*, vol. 37(1), pp. 73–85, 2009,doi: 10.1080/15397730802713389.

[11] Y.M. Al-Smadi, K.Russell, and R.S. Sodhi, "On traveler braking mechanism design with elastic deflection and buckling considerations," *Mech. Based Des. Struct. Mach.*, vol. 37, no. 3, pp. 401–412, 2009, doi: 10.1080/15397730902970483.

[12] S. Mutawe, Y.M. Al-Smadi, and R.S. Sodhi, "Planar four-bar path generation considering worst case joint tolerances," *Proc. World Congr.*, vol. I, no. 1, pp. 2–6, 2011.

[13] G.P. Roston, and R.H. Sturges, "Genetic algorithm synthesis of four-bar mechanisms," *Artificial Intelligence for Engineering Design, Analysis and Manufacturing*, vol. 10, no. 5, pp. 371–390, 1996, doi: 10.1017/s0890060400001700.
[14] J.A. Cabrera, A. Simon, and M. Prado, "Optimal synthesis of mechanisms with genetic algorithms," *Mech. Mach. Theory*, vol. 37, no. 10, pp. 1165–1177, 2002, doi: 10.1016/s0094-114x(02)00051-4.
[15] S.S. Shete, and S.A. Kulkarni, "Dimensional synthesis of four bar mechanism using genetic algorithm," *Int. J. Eng. Res.*, vol. 4, no. 3, pp. 123–126, 2015, doi: 10.17950/ijer/v4s3/308.
[16] P. Bajpai, "Genetic algorithm – an approach to solve global optimization problems," *J. Comput. Sci. Eng*., vol. 1, no. 3, pp. 199–206, 2016.
[17] W. E. Fang, "Simultaneous type and dimensional synthesis of mechanisms by genetic algorithms," *Mechanism Synthesis and Analysis*, vol. 70, pp. 35-41, 1994.
[18] S. K. A. Kunjur, "Genetic algorithms in mechanical synthesis, " J*ournal of Applied Mechanisms and Robotics*, vol. 4, no. 2, pp. 18–24, 1997.
[19] W.Y. Lin, "A GA–DE hybrid evolutionary algorithm for path synthesis of four-bar linkage," *Mech. Mach. Theory*, vol. 45, no. 8, pp. 1096–1107, 2010, doi: 10.1016/j.mechmachtheory.2010.03.011.
[10] M.A. Laribi, A. Mlika, L. Romdhane, and S. Zeghloul., "A combined genetic algorithm–fuzzy logic method (GA–FL) in mechanisms synthesis," *Mech. Mach. Theory*, vol. 39, no. 7, pp. 717–735, 2004, doi: 10.1016/j.mechmachtheory.2004.02.004.
[21] C.H. Suh and C. W. Radcliffe, *Kinematics & Mechanisms Design*, John Wiley&Sons, 1978.
[22] A. Rahmani Hanzaki, P.V.M. Rao, and S.K. Saha, "Kinematic and sensitivity analysis and optimization of planar rack-and-pinion steering linkages," *Mech. Mach. Theory,* vol. 44, no. 1, pp. 42–56, 2009, doi: 10.1016/j.mechmachtheory.2008.02.014.
[23] A. Karamoozian *et al.*, "Sensitivity analysis of the equal angle divider mechanism kinematics with the synthesis of the joint gap tolerances," *Mech. Based Des. Struct. Mach.*, vol. 46, no. 4, pp. 499–519, 2018, doi: 10.1080/15397734.2017.1362984.
[24] R. Sancibrian, P. Garcia, F. Viadero, A. Fernandez, "Optimal synthesis of linkages using sensitivity coefficients in path generation problems," I*ASME Transactions,* vol. 1, no. 1, pp. 114-119, 2004.
[25] S. Faik, and A.G. Erdman, "Sensitivity distribution in the synthesis solution space of four-bar linkages," *J. Mech. Des.*, vol. 113(1), pp. 3–9, 1991, doi: 10.1115/1.2912748.
[26] P.S. Shiakolas, D. Koladiya, and J. Kebrle, "On the optimum synthesis of four-bar linkages using differential evolution and the geometric centroid of precision positions," *Inverse Probl. Sci. Eng.*, vol. 10(6), pp. 485–502, 2002, doi: 10.1080/1068276021000054594.
[27] Y. M. Al-Smadi, K. Russell, and R.S. Sodhi, "Four-bar motion generation with elasticity constraints and optimization," *Proc. Inst. Mech. Eng., Part K, J. Multi-body Dynamics*, vol. 223, no. 3, pp. 245–253, 2009.
[28] J. Angeles, *Fundamentals of robotic mechanical systems*, Springer International Publishing, 2014.
[29] B. M Oraik, N. Zamri, and Y. M. Al-Smadi, "Inverse kinematic synthesis of motion generation four-bar stamping mechanism," *Int. J. Recent Technol.* (IJRTE), vol. 8, no. 1, pp. 771-776, 2019.